

On Synchronization and Control of Coupled Wilson-Cowan Neural Oscillators

Tetsushi Ueta * Guanrong Chen †

Abstract

This paper investigates the complex dynamics, synchronization, and control of chaos in a system of strongly connected Wilson-Cowan neural oscillators. Some typical synchronized periodic solutions are analyzed by using the Poincaré mapping method, for which bifurcation diagrams are obtained. It is shown that topological change of the synchronization mode is mainly caused and carried out by the Neimark-Sacker bifurcation. Finally, a simple feedback control method is presented for stabilizing an in-phase synchronizing periodic solution embedded in the chaotic attractor of a higher-dimensional model of such coupled neural oscillators.

1 Introduction

Oscillatory behavior is a fundamental phenomenon in physical, chemical, electronic, and biological systems. A complex system consisting of a set of massive and connected oscillatory cells or particles can be considered as a large-scaled network of coupled oscillators, and they are synchronized together under certain conditions. For instance, synchrony of a population of flashing fireflies provides a typical and interesting example of synchronization phenomenon [Strogatz & Stewart, 1994].

The human brain activity is usually modeled by a coupling network of cells, namely, a complex system with massive neurons. One way to understand such complicated dynamical behaviors of a complex system is to decompose it into small oscillatory units and then perform some analysis on their oscillatory modes at the lower-dimensional scale from a physical point of view. To that end, the entire system can be better understood. This strategy has been applied to brain analysis, by reducing its model dimension so that an averaged behavior in a local population of neurons can be studied. Hoppensteadt and Izhikevich [Hoppensteadt & Izhikevich, 1997] provided some qualitative analysis on periodic solutions and their synchronization in a special coupled neurons, called the Wilson-Cowan model. More precisely, they studied the phase equation derived from a limit cycle of the coupled neurons, and applied the averaging method for its analysis. Note that this can be done under an assumption – the coupling strength is weak. However, it is more interesting to investigate what happens if such a coupling effect is strong.

*Department of Information Science and Intelligent Systems, Tokushima University, Tokushima, 770-8506 Japan
tetsushi@is.tokushima-u.ac.jp

†Department of Electrical and Electronic Engineering, City University of Hong Kong, Hong Kong, P. R. China
gchen@ee.cityu.edu.hk

It has been widely experienced that even a small-scale and simplified model can exhibit a rich variety of complex behaviors if the coupling effect is strong. For this situation, an analytical approach to the analysis becomes very difficult, if not impossible. This is especially true for brain neurons where the coupling effect is strong. In this case, numerical study is virtually the only possible choice for analysis.

In this paper, we study the complex dynamical behaviors of a coupled neural model of oscillators with strong coupling effects. The Wilson-Cowan model is chosen as an oscillator in the network, and we mainly focus our attention on the study of two coupled oscillators. First, we study the stability of periodic solutions and, then, obtain their bifurcation diagram. In-phase and out-phase synchronized solutions, as well as symmetric periodic solutions, are completely classified by the bifurcation diagram. The parameter region where the system behaves chaotically is also clarified. Then we show that the Neimark-Sacker bifurcation plays an important role in this coupled neuron system. We identify a new type of intermittency response, and show that this response reflects spatio-temporal behaviors in higher-dimensional systems. Finally, we discuss how to stabilize an unstable synchronized periodic orbit embedded in the chaotic region, by using continuous state feedback. As an example, chaos in six coupled oscillators is controlled to their in-phase synchronization.

2 Mathematical Model of the Wilson-Cowan Network

The dynamics of a continuous-time neural network can be described by the following system of differential equations:

$$\dot{x}_i = -\alpha_i x_i + f\left(\rho_i + \sum_{j=1}^n c_{ij} x_j\right), \quad x_i \in \mathbf{R}, \quad i, j = 1, \dots, n, \quad (1)$$

where all coefficients are constants, with $\alpha_i \geq 0$, and f is a sigmoid function defined by

$$f(x) = \frac{1}{1 + \exp(-\epsilon x)}, \quad \epsilon > 0. \quad (2)$$

In case that n is a big number, such a model has rich variety of oscillatory behaviors, various (in-phase, out-phase, or n -phase) synchronizations, tori, bifurcations and chaos, etc.

In [Wilson & Cowan 1973], a model of neural oscillators, probably the simplest of its kind, is developed by considering a specific case of Eq. (1), namely,

$$\begin{aligned} \dot{x} &= -\alpha x + f(ax - by + \rho_x) \\ \dot{y} &= -\beta y + f(cx - dy + \rho_y). \end{aligned} \quad (3)$$

This model describes the coupling of an excitatory and an inhibitory neuron via synapses, as illustrated by Fig. 1 (a).

System (3) has some typical bifurcation phenomena, such as the saddle-node and Hopf bifurcations from an equilibrium, generation and saddle connection of limit cycles, and other degenerate bifurcations [Hoppensteadt & Izhikevich, 1997][Borisyk, et al., 1995]. The bifurcation structure of Eq. (3) in the ρ_x - ρ_y plane is somewhat similar to an averaged system of the van der Pol or the Duffing-Rayleigh oscillator. Therefore, coupled neurons can be thought of as a nonlinear oscillator. However, a network consisting of more than two such oscillators may not be assumed to be a mutually coupled system.

This issue is different from the familiar coupled electric circuits, because the synaptic coupling here is one-directional and the coupling term is contained inside the sigmoid function f .

In [Hoppensteadt & Izhikevich, 1997], weakly connected neural networks are studied via some analytical (averaging) methods under the assumption that the synaptic coefficients are small. In this paper, we instead attempt to investigate coupled neural oscillators with strong synaptic connections. One motivation is that a strong coupling between two neurons in biophysical signaling mechanisms is very common, at least in many artificial neural networks (i.e., perceptions, recurrent neural networks, and cellular neural networks [Thiran, 1997]).

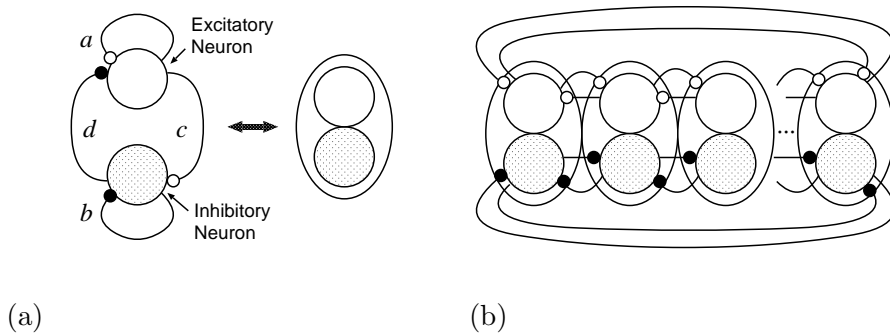


Figure 1: (a) Coupled neurons. (b) A ring configuration.

Observe that for a coupling configuration among all oscillators, the connections “excitatory \rightarrow excitatory” and “inhibitory \rightarrow inhibitory” are essential for in-phase and out-phase synchronizations [Hoppensteadt & Izhikevich, 1997]. Therefore, we are interested in considering this kind of coupling structure, on the change of its synchronizing modes, as the coupling coefficient is increased.

Figure 1 (b) shows a ring-configuration of such coupled neural oscillators. The corresponding system of equations are

$$\begin{aligned} \dot{x}_i &= -\alpha x_i + f(ax_i - by_i + \rho_x + \delta_x(x_{i-1} + x_{i+1})) \\ \dot{y}_i &= -\beta y_i + f(cx_i - dy_i + \rho_y - \delta_y(y_{i-1} + y_{i+1})) \\ i &= 1, 2, \dots, n \pmod{n}, \end{aligned} \tag{4}$$

where $\alpha > 0$, $\beta > 0$, and $a, b, c, d, \rho_x, \rho_y, \delta_x$, and δ_y are constants.

We are interested in the global behaviors of these two strongly coupled oscillators.

3 Periodic Solutions and Chaos

In this section, we investigate the characteristics of the periodic solutions in the ring-configuration of the coupled oscillators. In each individual oscillator, described by Eq. (3), we fix the parameter values to be

$$\alpha = \beta = 1, \quad \epsilon = 1, \quad a = b = 10, \quad d = -2, \quad \rho_x = 0, \quad \rho_y = -6.$$

Based on a typical analysis about the equilibria of the above system, we can calculate the Hopf bifurcation parameter and obtain $c = 6.62$. Then, we know that there are an unstable equilibrium and a stable limit cycle in the two-dimensional system. These repeller and attractor are created right after the Hopf bifurcation at a stable equilibrium.

3.1 The Poincaré Map and Calculation of Bifurcation Parameters

Consider a general nonlinear autonomous system of the form

$$\frac{d\mathbf{x}}{dt} = \mathbf{f}(\mathbf{x}, \lambda), \quad \mathbf{x} \in \mathbf{R}^n, \quad \lambda \in \mathbf{R}, \quad (5)$$

where \mathbf{f} is a C^∞ function, and λ is a real parameter. Suppose that system (5) has a solution φ , starting from an initial point, \mathbf{x}_0 :

$$\mathbf{x}(t) = \varphi(t, \mathbf{x}_0), \quad \mathbf{x}(0) = \varphi(0, \mathbf{x}_0) = \mathbf{x}_0.$$

Also, assume that there is a limit cycle of period $\tau > 0$ for an appropriate parameter value:

$$\varphi(\tau, \mathbf{x}_0) = \varphi(0, \mathbf{x}_0).$$

By placing the Poincaré section Π , described by a scalar function q , to the limit cycle transversely, we obtain

$$\Pi = \{ \mathbf{x} \in \mathbf{R}^n \mid q(\mathbf{x}) = 0 \}. \quad (6)$$

Thus, we can define the Poincaré map T as follows:

$$\begin{aligned} T: \Pi &\rightarrow \Pi \\ \mathbf{x} &\mapsto \varphi(\tau(\mathbf{x}), \mathbf{x}). \end{aligned} \quad (7)$$

To reduce the dimension of this map, we introduce the local coordinates

$$\mathbf{u} \in \Sigma \subset \mathbf{R}^{n-1},$$

with a projection and an embedding map:

$$h: \Pi \rightarrow \Sigma, \quad h^{-1}: \Sigma \rightarrow \Pi.$$

Thereby we obtain the Poincaré map T_ℓ on the local coordinates, such that

$$\begin{aligned} T_\ell: \Sigma &\rightarrow \Sigma \\ \mathbf{u} &\rightarrow h \circ T \circ h^{-1} = h(\varphi(\tau(h^{-1}(\mathbf{u})), h^{-1}(\mathbf{u}))). \end{aligned} \quad (8)$$

In general, a point \mathbf{u}_0 satisfying

$$\mathbf{u}_0 = T_\ell(\mathbf{u}_0) \quad (9)$$

is called a *fixed point of the map* (to distinguish it from an *equilibrium point of the system*) in this paper. The stability of this fixed point is determined by the multipliers (roots) of the characteristic equation for the Jacobian of system (7) (see [Ueta et al., 1997] for more details):

$$\chi(\mu) := \det(DT - \mu I_n) = 0, \quad (10)$$

where I_n is the $n \times n$ identity matrix.

To obtain bifurcation parameter values, we have to solve Eqs. (6), (9), and (10), for \mathbf{u}_0 , λ , and τ , simultaneously.

3.2 A Simple Coupled-Neuron Model

Now, we focus our attention on a simple pair of coupled neurons:

$$\begin{aligned}
 \dot{x}_1 &= -x_1 + f(ax_1 - by_1 + \rho_x + \delta x_2) \\
 \dot{y}_1 &= -y_1 + f(cx_1 - dy_1 + \rho_y - \delta y_2) \\
 \dot{x}_2 &= -x_2 + f(ax_2 - by_2 + \rho_x + \delta x_1) \\
 \dot{y}_2 &= -y_2 + f(cx_2 - dy_2 + \rho_y - \delta y_1).
 \end{aligned} \tag{11}$$

This model has a limit cycle, and the Neimark-Sacker (NS) bifurcation occurs under a certain condition. After this bifurcation, the limit cycle changes its behavior to be quasi-periodic, phase-locking, and torus breakdown, as the connection coefficient δ is increased.

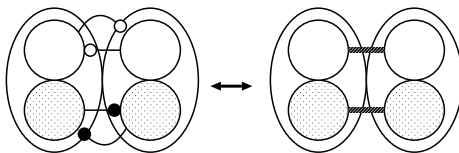


Figure 2: Coupled neuron oscillators and the abbreviation.

We examine this system dynamics on the c - δ plane. First, choose the Poincare section $\Pi = \{\mathbf{x} \mid x_1 - x_1^* = 0\}$, where x_1^* is the x -coordinate value of the fixed point \mathbf{x}^* . Limit cycle in this system is generated by the Hopf bifurcation of the equilibrium point \mathbf{x}^* . Therefore, Π , which contains the point \mathbf{x}^* , is adequate to be used as a transversal section.

Symmetry plays an important role in this system. For instance, we can easily see that the permutation

$$P : \mathbf{R}^4 \rightarrow \mathbf{R}^4; (x_1, y_1, x_2, y_2) \mapsto P(x_1, y_1, x_2, y_2) = (x_2, y_2, x_1, y_1)$$

is invariant for Eq. (11). A permutation P can be written as

$$P = \begin{pmatrix} 0 & I_2 \\ I_2 & 0 \end{pmatrix},$$

where I_2 is the 2×2 identity matrix. Let the system (11) be written in the form of (5). If the right-hand side of Eq. (5) has the following relationship, then the equation is said to be P -symmetric:

$$\mathbf{f}(P\mathbf{x}) = P\mathbf{f}(\mathbf{x}).$$

Due to this symmetry of the equation, all periodic solutions of the system have symmetrical properties. There typically exist three types of periodic solutions:

- in-phase synchronization (IN);
- almost out-phase synchronization (OUT);
- symmetric periodic solution (S).

Table 1: Typical local bifurcations for limit cycles (k is an integer).

Bifurcation	Symbol	Change of fixed points
Tangent	T	${}_kD + {}_{k+1}D \iff \emptyset$
Period-doubling	Pd	${}_kD \iff {}_{k+1}I + 2 \times {}_kD^2$
Neimark-Sacker	NS	${}_kD \iff {}_{k+2}D + \text{torus}$
Pitchfork-I	Pf	${}_kD \iff {}_{k+1}D + 2 \times {}_kD$
Pitchfork-II	Pf	${}_kD \iff {}_{k-1}D + 2 \times {}_kD$

For the IN solution, we have

$$\varphi(t, \mathbf{x}_0) = P\varphi(t, \mathbf{x}_0).$$

In this case, we always have $x_1(t) = x_2(t)$ and $y_1(t) = y_2(t)$, for all t . This means that both neural oscillators are completely synchronized without delay.

The OUT solution can be regarded as an almost out-phase synchronized solution for each oscillator, namely, it has a half-period delay between the two oscillators. Actually, this solution satisfies

$$\varphi(\tau/2, \mathbf{x}_0) = P\mathbf{x}_0,$$

where τ is the period.

For the solution S, there exist a pair of symmetric solutions, $\varphi_1(t)$ and $\varphi_2(t)$, satisfying

$$\varphi_1(t, \mathbf{x}_0) = P\varphi_2(t, P\mathbf{x}_0), \quad \varphi_2(t, \mathbf{x}_0) = P\varphi_1(t, P\mathbf{x}_0). \quad (12)$$

These solutions are generated by a pitchfork bifurcation of the IN solution.

Stabilities of periodic solutions are determined by the multipliers of the characteristic equation for the fixed point. We denote these stabilities by indexes ${}_kD$ or ${}_kI$, with D and I indicating the orientation preserving and reversing maps on the unstable eigenspace of dimension k , respectively [Kawakami, 1984].

Figure 3 (a) shows an example of the phase portrait (a projection of x_1 - x_2) of the co-existing periodic solutions. In this figure, we can see the phase differences between the two oscillators. For instance, $\text{IN}({}_0D)$ is a stable in-phase synchronized solution since the state is always located on the diagonal $x_1 = x_2$. On the other hand, $\text{OUT}({}_2D)$ indicates a two-dimensionally unstable and almost out-phase synchronized solution, as shown in Fig. 3 (b). Moreover, $\text{S}_1({}_1D)$ and $\text{S}_2({}_1D)$ are one-dimensionally unstable saddles, and they are symmetrical about the diagonal $x_1 = x_2$ and is affected by the relationship (12).

For system (11), bifurcation phenomena can be classified into five types, as summarized in Table 1. In this table, \emptyset indicates the disappearance of fixed points, and index ${}_0D^2$ indicates a two-periodic point for index ${}_0D$.

Next, we show a bifurcation diagram in the c - δ parameter plane (see Fig. 4). In Fig. 4 (b), each segment separated by the bifurcation curve has different topological properties of the corresponding periodic solutions. These segments are labeled by numbers (1)–(12), and their corresponding solutions

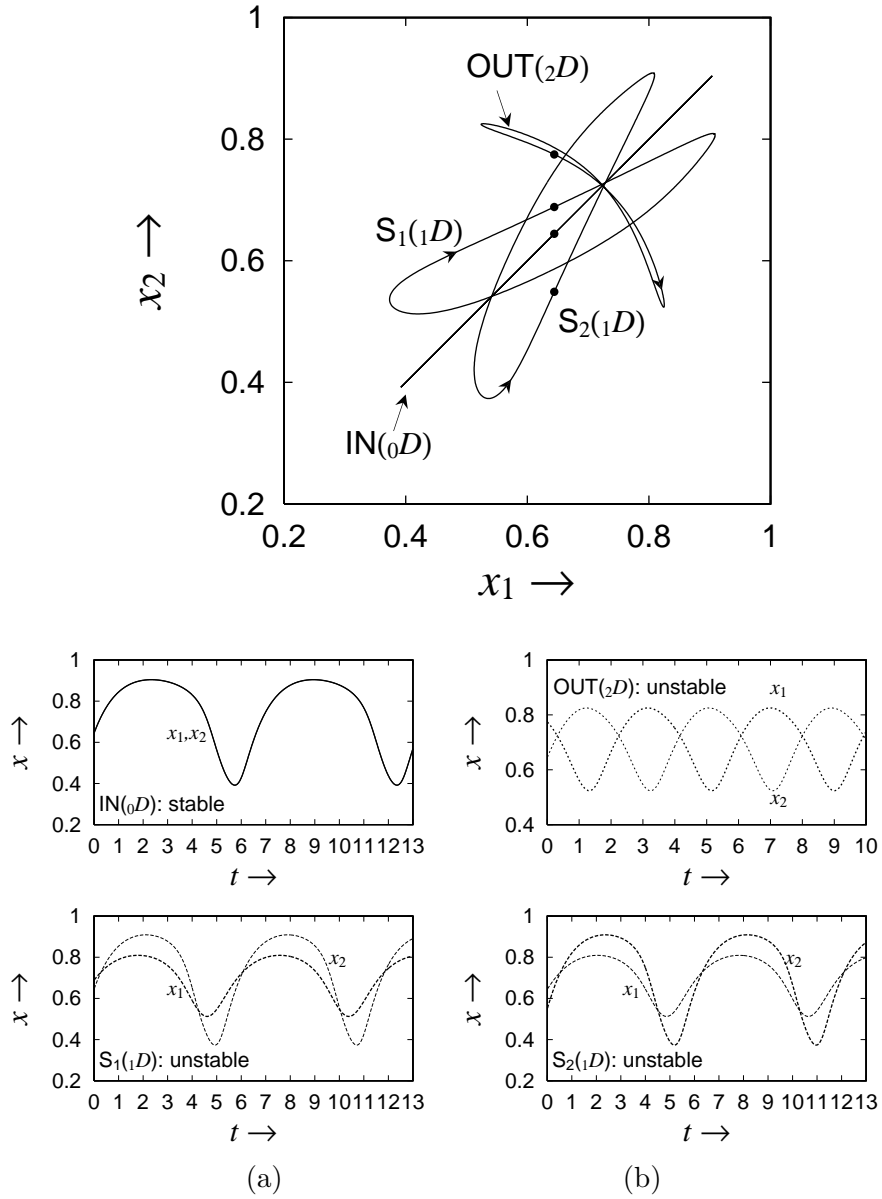
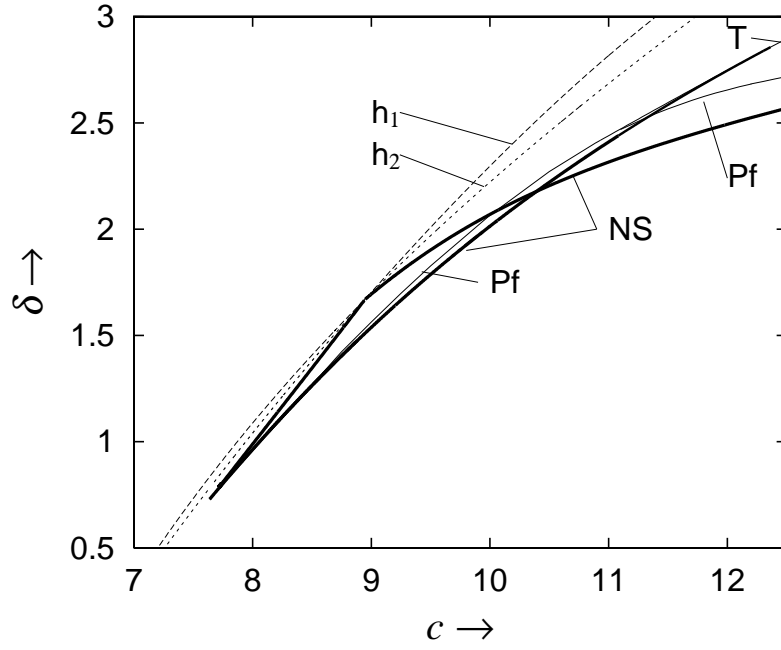
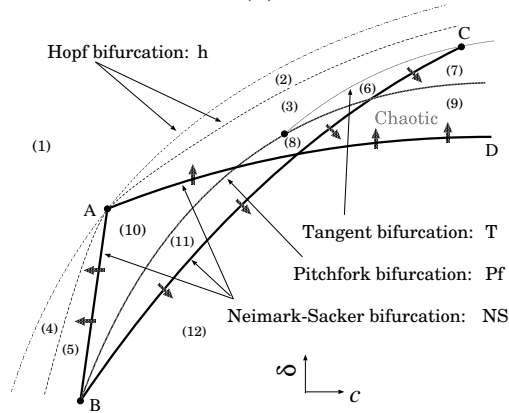


Figure 3: Co-existence of solutions. $c = 12.0$, $\delta = 2.747$. Black circles are fixed points of the Poincaré map.



(a)



(b)

Figure 4: Bifurcation diagram (a) and its schematic diagram (b). $a = b = 10$, $d = -2$, $\rho_x = 0$, $\rho_y = -6$.

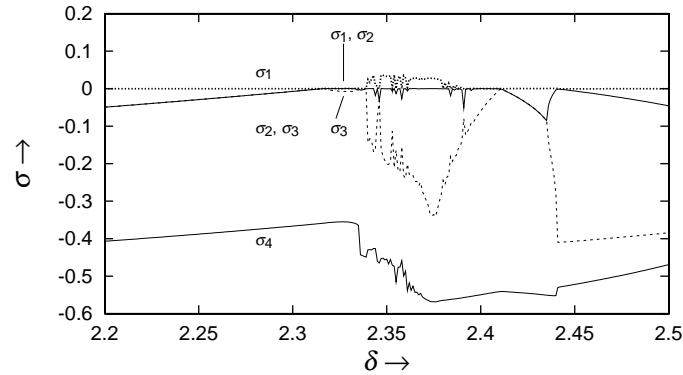
are listed below:

- (1) \emptyset
- (2) $\text{IN}(0D)$
- (3) $\text{IN}(0D) + \text{OUT}(2D)$
- (4) $\text{OUT}(0D)$
- (5) $\text{IN}(2D) + \text{OUT}(0D)$
- (6) $\text{IN}(0D) + \text{OUT}(2D) + 2 \times \text{S}(0D) + 2 \times \text{S}(1D)$
- (7) $\text{IN}(0D) + \text{OUT}(2D) + 2 \times \text{S}(2D) + 2 \times \text{S}(1D)$
- (8) $\text{IN}(1D) + \text{OUT}(2D) + 2 \times \text{S}(0D)$
- (9) $\text{IN}(1D) + \text{OUT}(2D) + 2 \times \text{S}(2D)$
- (10) $\text{IN}(0D) + \text{OUT}(0D)$
- (11) $\text{IN}(1D) + \text{OUT}(0D) + 2 \times \text{S}(0D)$
- (12) $\text{IN}(1D) + \text{OUT}(0D) + 2 \times \text{S}(2D)$

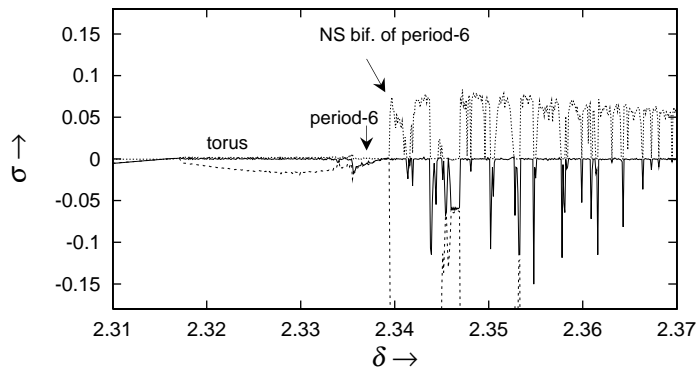
In area (1), there exists only one stable equilibrium. After crossing two Hopf bifurcations (h_1 and h_2), the equilibrium changes to a completely (four-dimensionally) unstable one. The S-type of solutions are created by a pitchfork bifurcation (Pf) for an IN type of solution. In area (8), only two S-type of solutions are observed, which are stable in the large.

Next, we focus on the Neimark-Sacker (NS) bifurcations. In Fig. 4 (b), the half lines \overline{AB} , \overline{AD} , and \overline{BC} are NS bifurcations of the IN, OUT, and S-types of solutions, respectively. Thick arrows indicate that tori are generated by changing parameter values along the corresponding direction. In areas (7) and (9), many periodic solutions (without a symmetrical property) and tori co-exist, and they eventually collapse to chaos. There is no area in which IN, OUT, S solutions co-exist as stable orbits; IN and OUT solutions are observed to be stable only in area (10), depending on initial conditions. From these diagrams and the above classification, the change between IN and OUT synchronizations is clarified.

Figure 5 shows the system Lyapunov exponents for the parameter range $2.2 < \delta < 2.5$, with $c = 11$. In the case of $\delta < 2.314$, there is an $\text{IN}(0D)$ solution. At $\delta \approx 2.314$, an NS bifurcation occurs, then a quasi-periodic solution (torus) is generated, see Fig. 6 (a). This can be confirmed by the fact that it has double zero Lyapunov exponents. For the parameter range $2.334 < \delta < 2.336$, a torus and many periodic attractors are alternatively observed (frequency locking). When $\delta \approx 2.335$, the system has a chaotic transient starting from an arbitrary initial value within this parameter range. After the chaotic transient, the torus is broken and the orbit is absorbed by those periodic attractors. A period-8 attractor then appears, see Fig. 6 (b). By a slight increase in the value of δ , this attractor meets cascade period-doubling bifurcations. After that, periodic and chaotic responses are observed within a very narrow range of parameter values (with slight perturbations). When $\delta \approx 2.336$, a period-6 attractor emerges. The Neimark-Sacker bifurcation for this attractor is caused at $\delta \approx 2.339$ and, after this bifurcation, the generated torus is immediately absorbed into a co-existing chaotic attractor. Beyond the range of chaos, many periodic windows are observed. We found period-doubling bifurcations for some periodic solutions within these windows. We also observe the torus precisely with $c = 13$, $2.7 < \delta < 2.8$. Figure 7 show the Lyapunov exponents. A torus generated by the Neimark-Sacker bifurcation is shown in Fig. 7 (a). As δ increases from 2.7, the torus is gradually distorted, see

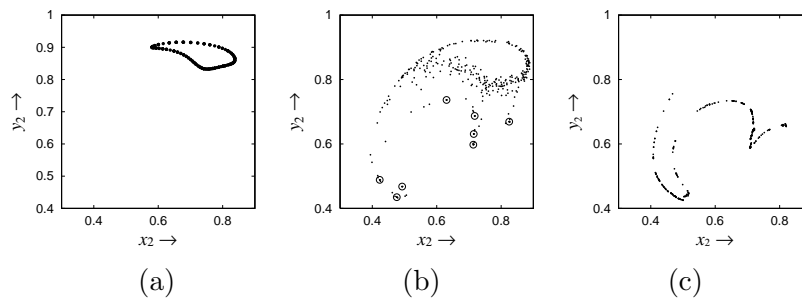


(a)



(b)

Figure 5: Lyapunov exponents. $c = 11$. (a) all exponents, (b) enlargement of (a).



(a)

(b)

(c)

Figure 6: The Poincaré map in the x_2 - y_2 plane. $c = 11$. (a) A torus. $\delta = 2.32$ (b) $\delta = 2.339$. The torus is broken, and the orbit behaves chaotically for a while; finally, it is trapped into eight-periodic points (marked by circles). (c) A chaotic attractor. $\delta = 2.34$.

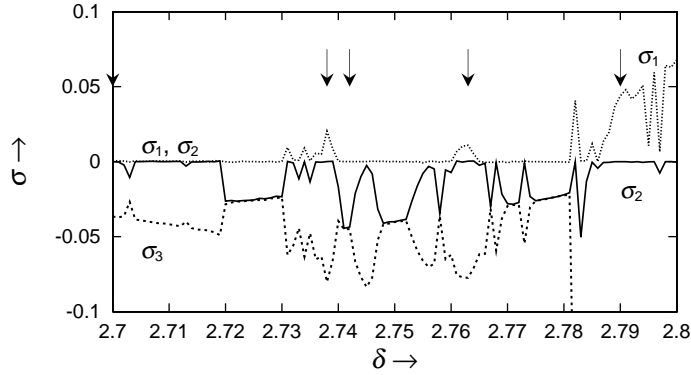


Figure 7: Lyapunov exponents near torus breakdown. $c = 13$.

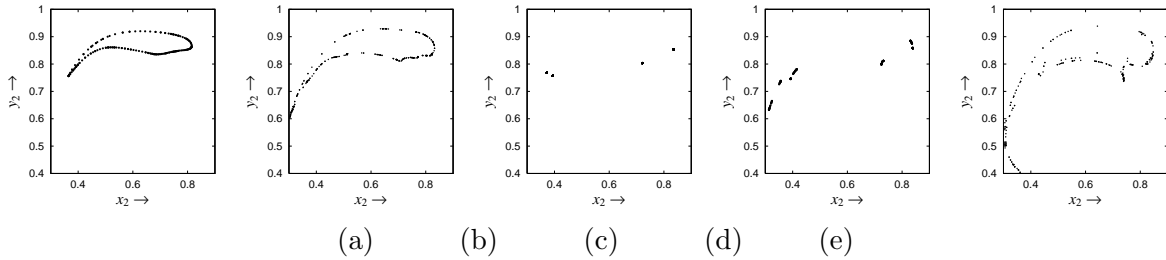


Figure 8: Phase portraits according to parameter values indicated in Fig. 7. (a) torus, $\delta = 2.7$. (b) chaotic, $\delta = 2.738$. (c) 4-periodic locking, $\delta = 2.742$. (d) chaos via cascade period-doubling for a period-4 solution, $\delta = 2.763$. (e) chaos, $\delta = 2.79$.

Fig.7 (b), and frequently trapped into periodic locking regions, see Fig. 7 (c). Such periodic solutions become an “islet” chaotic attractor via period-doubling cascade, see Fig. 7 (d), and, sometimes, the solution forms a folded torus, see Fig. 7 (e). From these observations, we conclude that a typical torus-breakdown scenario [Matsumoto et al., 1993] exists in this system of coupled neurons.

3.3 Intermittency Responses

After a pitchfork bifurcation of $IN(0D)$ (in area (6) or (7) of Fig. 4), we observe two saddle-type periodic solutions, $S(1D)$ s. Under certain initial conditions, we see a novel intermittency response: the orbit stays for a while near one of the two $S(1D)$ s (since an $S(1D)$ has two stable manifolds and one unstable manifold whose corresponding multiplier is slightly larger than unity). Thus, after temporally staying at $S(1D)$, the orbit escapes from $S(1D)$. However, the orbit is immediately trapped into another $S(1D)$ after a very short chaotic transient, and behaves periodically for a while again, as shown in Fig. 9 (a). This switching between the two $S(1D)$ s are permanent, but each staying time at either $S(1D)$ cannot be estimated, perhaps due to the chaotic nature of the motion (in fact, the maximum Lyapunov exponent of this attractor is $+0.07$).

This kind of intermittency is not related to tangent, period-doubling (flip), or the NS bifurcation. Instead, it is related to pitchfork bifurcation. This phenomenon is not conformed to the types I–III

intermittency classified in [Pomeau and Manneville, 1980]. Figure 9 shows the manifolds of an $S(1D)$. The Poincaré maps are slightly closer to the unstable manifold of the $S(1D)$. Note that there also exists an $IN(0D)$ (stable) solution at this parameter value, but it has another basin of attraction. Thus, this intermittency response can be everlastingly observed.

Similar phenomenon can be observed in the case of higher-dimensional ring-configuration of coupled oscillators. Figure 10 shows some peculiar wave forms of six coupled oscillators. There are two oscillations of different amplitudes where the switching between these oscillators is chaotic. This phenomenon is also due to the intermittency response of $S(1D)$ s. In this figure, we can see a temporal in-phase synchronization between two states of the system in a short period of time.

3.4 Coalesce of Tori

As another impressive phenomenon related to the S solution, coalesce of tori (torus symmetry breaking bifurcation) is observed from Eq. (11), see also Fig. 11. This phenomenon was also found in another type of coupled neural oscillators [Borisyyk, et al., 1995].

Two tori in Fig. 11 (a) are caused by crossing the NS bifurcation for $S(0D)$ from area (11) to area (12) in Fig. 4. In area (12), near the NS bifurcation curve \overline{BC} , there exist an unstable saddle $IN(1D)$, a stable sink $OUT(0D)$, and two $S(2D)$ s with two stable tori. The tori approach each other as the parameter δ decreases. In Fig. 11 (c), they are coalesced with the saddle orbit, and finally a torus is generated and the saddle is separated from the torus as shown in Fig. 11 (d). Note that the NS bifurcation for the IN-type solution (curve \overline{AB}) does not affect this phenomenon.

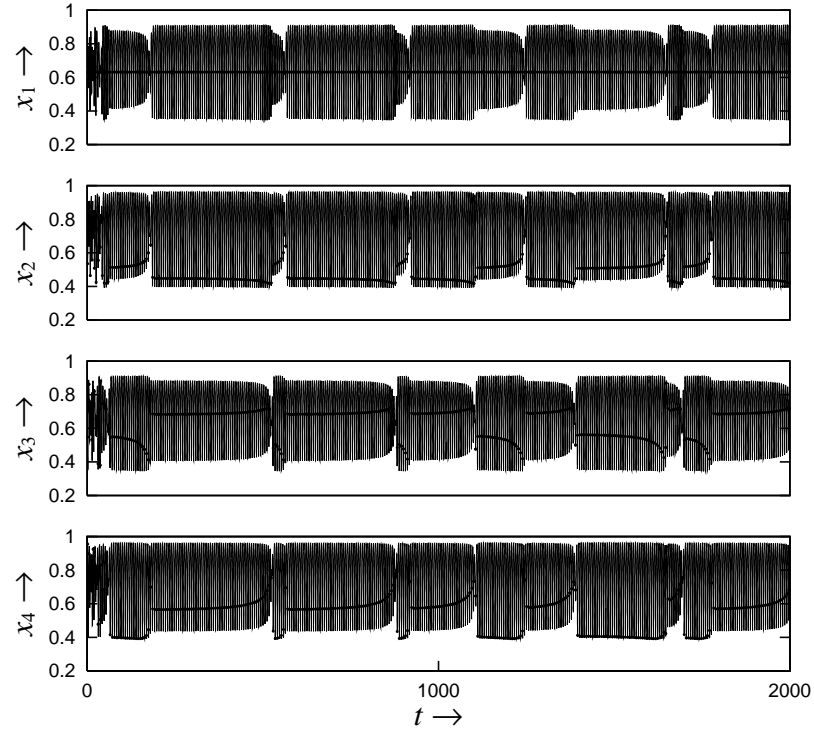
In general, in nonlinear systems these tori meet with torus-breakdown and are changed to chaotic solutions just before coalescing. To clarify this coalesce of plain tori, it is important to examine the manifolds of the saddle $IN(1D)$. This remains as an intensive research problem for future studies.

4 Controlling to Unstable Periodic Orbits

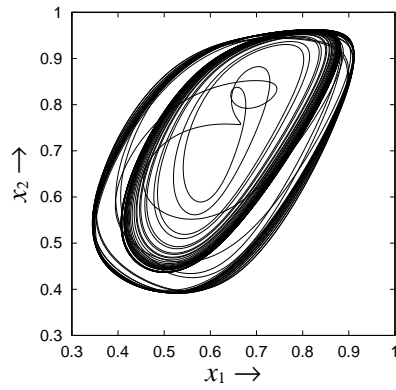
For some practical applications of artificial neural networks in information processing, such as solving optimization problems and searching for associative memory, chaos seems to be effective. In many other applications, however, chaotic system trajectories have to be stabilized, for example to an unstable periodic orbit (UPO) embedded in the chaotic attractor [Chen, 1999, Chen & Dong 1998, Ueta et al., 2001]. In particular, controlling UPOs is one of the many significant problems for neural networks [Mizutani et al., 1998].

In this section, we discuss how a UPO embedded in a chaotic attractor of the coupled-neuron model can be stabilized via feedback control. Since the mathematical model is known, we can calculate its bifurcation parameter values or fixed/periodic points, by using the Poincaré map and related analytic methods mentioned in Section 3.1, even though the target periodic solution is unstable.

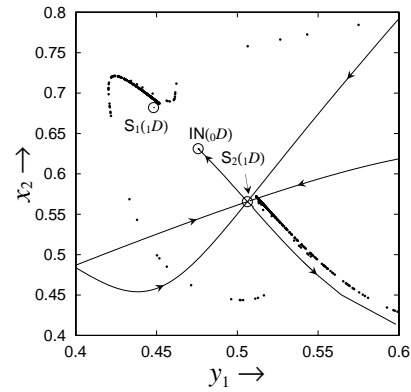
In this attempt, the time-delayed feedback control [Pyragas, 1992] turns out to be suitable, since we have accurate information about the target UPO, which is used as the reference signal. Differing from [Pyragas, 1992], we feed the control input (stimuli) into the sigmoid function f based on the additive neural dynamics (see Eq. (1) for a reason).



(a)



(b)



(c)

Figure 9: Intermittency response at $c = 12$ and $\delta = 2.668$. (a) Time response with an arbitrary initial condition. Small black circles are the Poincaré section points. (b) Phase portrait in the x_1 - y_1 plane. (c) Stable and unstable manifolds of $S_2(1D)$.

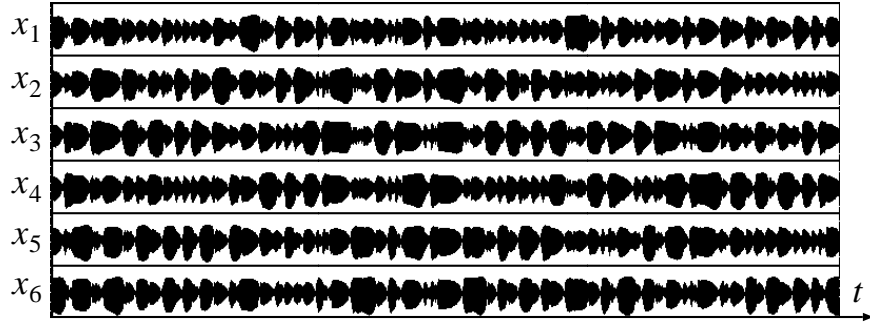


Figure 10: A snapshot of the wave form x_i in six coupled-neurons. $c = 10$, $\delta = 1.09$, $1000 < t < 6000$. The average value of return time for a cycle is about 6.14 sec.

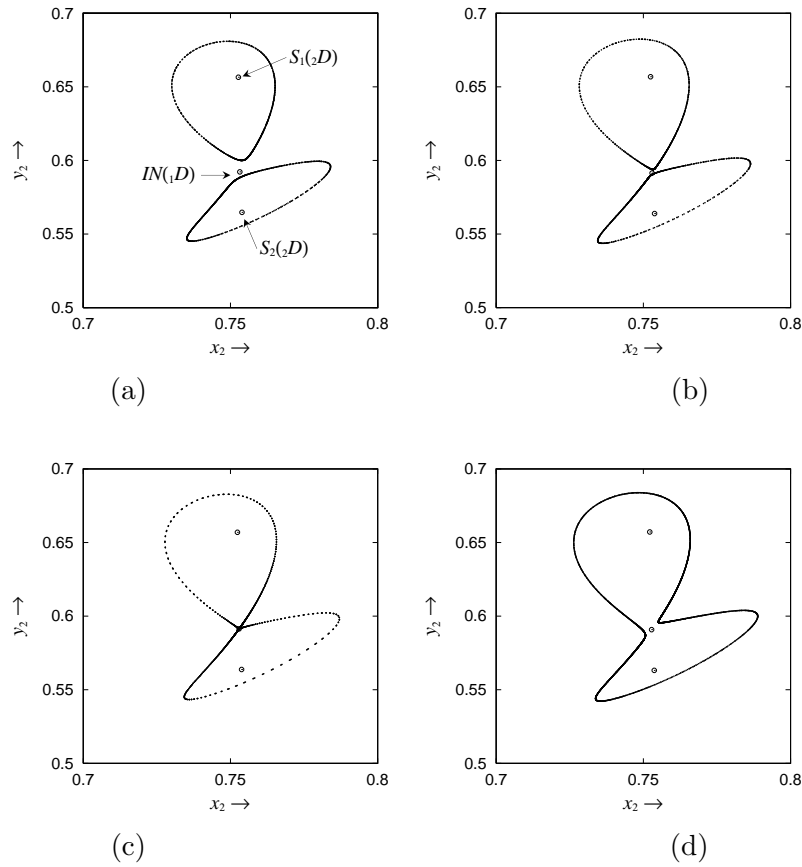


Figure 11: Coalesce of tori. All points are projections of the Poincaré map on the x_2 - y_2 plane. (a): $\delta = 1.529$. (b): $\delta = 1.528$, (c): $\delta = 1.52774$, (d): $\delta = 1.527$, $a = b = 10$, $c = 9$, $d = -2$, $\rho_x = 0$, $\rho_y = -6$.

For simplicity, the control is added only to the x -components of the system. Thus, the controlled system is

$$\begin{aligned}\dot{x}_i &= -x_i + f(ax_i - by_i + \rho_x + \delta(x_{i-1} + x_{i+1}) + K(x_i^* - x_i)) \\ \dot{y}_i &= -y_i + f(cx_i - dy_i + \rho_x - \delta(y_{i-1} + y_{i+1})), \quad i = 1, 2, \dots, n,\end{aligned}$$

where x_i^* are the corresponding x -components of the UPO and $K > 0$ is a control gain to be determined (see Fig. 12).

In the previous section, we have seen the chaotic response in the case of six-oscillators, with $c = 10$ and $\delta = 1.09$ (Fig. 10). At these parameter values, there is a four-dimensionally unstable in-phase synchronized UPO (IN_(4D)). The maximum multiplier of this UPO is 1.2058 (double roots), and it is embedded within the chaotic attractor.

Figure 13 shows the time series of the controlled system response, where the control gain $K = 2.0$ was determined by trial-and-error. This control gain can also be determined by local stability analysis, which however is too conservative in general. Simulations have confirmed that by using conservative (sufficiently large) values of K , the control performance and its robustness can be remarkably improved.

Since we can accurately calculate the UPO by solving Eq. (9), this control method might work as well for any UPO by using a sufficient large value of K . Yet for a long-periodic UPO with high precision, a huge memory is needed to store the UPO data. In the case of stabilizing an in-phase synchronized oscillation in the ring-configuration of coupled oscillators, such memory is not needed in order to stabilize the UPO. That is, we can use the following equation as the reference oscillator:

$$\begin{aligned}\dot{x} &= -x + f((a + 2\delta)x - by + \rho_x) \\ \dot{y} &= -y + f(cx - (d + 2\delta)y + \rho_y).\end{aligned}$$

This equation is part of Eq. (4), with $x_{i-1} = x_i = x_{i+1}$ and $y_{i-1} = y_i = y_{i+1}$ therein. Using the x -component of the solution as the x^* of this equation, the same control performance has been verified. Figure 12 depicts this control scheme, and Fig. 13 shows its performance.

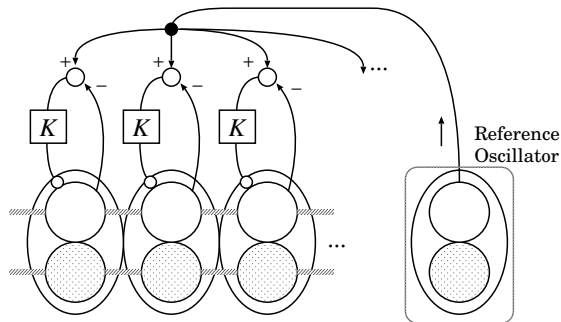
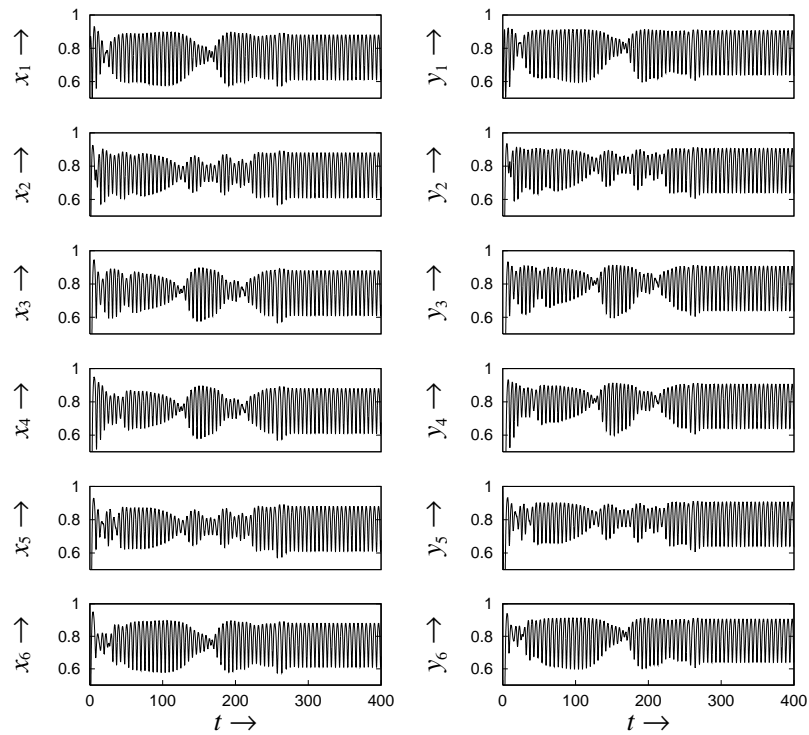


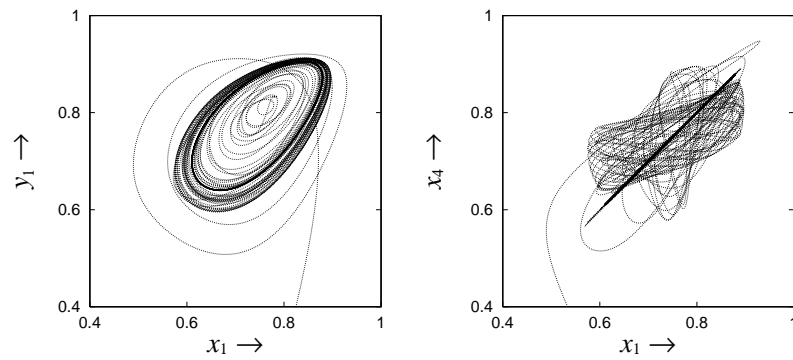
Figure 12: Coupled neurons with the controller for stabilization of in-phase synchronized orbits.

5 Concluding Remarks

In this paper, we have investigated the rich dynamical behaviors and a simple yet effective feedback chaos control method for a network of strongly connected neural oscillators. We have studied the



(a)



(b)

(c)

Figure 13: (a) Time response. The controller is turned on at $t = 250$. (b) x_1 - y_1 and (c) x_1 - x_2 phase portraits. Under control, the system states converge to the target orbit (thick curve).

existence and stability of some lower-dimensional system periodic orbits, and simulated some system bifurcation diagrams, chaotic motions, and synchronization phenomena. To this end, obtaining dynamic diagrams of higher-dimensional systems remains a great challenge for future research.

References

- [Borisyyk, et al., 1995] Borisyyk, G. N., Borisyyk, R. M., Khibnik A. I. and Roose, D. “Dynamics and bifurcations of two coupled neural oscillators with different connection types,” *Bulletin of Math. Biology*,, vol. 57, pp. 809–840, 1995.
- [Chen, 1999] Chen, G. “Chaos, bifurcations, and their control,” in J. Webster (Ed.), *Wiley Encyclopedia of Electrical and Electronics Engineering*, Wiley, New York, vol. 3, pp. 194–218, 1999.
- [Chen & Dong 1998] Chen G., and Dong, X. *From Chaos to Order: Methodologies, Perspectives and Applications*, World Scientific Pub. Co., Singapore, 1998.
- [Ermentrout & Cowan, 1980] Ermentrout, G. B., and Cowan, J. D. “Large scale spatially organized activity in neural nets,” *SIAM J. of Applied Mathematics*, vol. 38, pp. 1–21, 1980.
- [Hoppensteadt & Izhikevich, 1997] Hoppensteadt, F. C., and Izhikevich, E. M. *Weakly Connected Neural Networks*, Springer, AMS 126, 1997.
- [Izhikevich, 2000] Izhikevich, E. M. “Neural excitability, spiking and bursting,” *Int. J. Bifurcation and Chaos*, Vol. 10, No. 6, pp. 1171–1266, 2000.
- [Kawakami, 1984] Kawakami, H. “Bifurcation of periodic responses in forced dynamic nonlinear circuits,” *IEEE Trans. on Circ. Sys.*, vol. 31, pp. 248–260, 1984.
- [Matsumoto et al., 1993] Matsumoto, T., Komuro, M., Kokubu H. and Tokunaga, R. *Bifurcations*, Springer-Verlag, New York, 1993.
- [Mizutani et al., 1998] Mizutani, S., Sano, T., Uchiyama T. and Sonehara, N. “Controlling chaos in chaotic neural networks,” *Electronics and Communication in Japan*, Part 3, vol. 81, pp. 73–81, 1998.
- [Mpitsos et al., 1988] Mpitsos, G. J., Burton, R. M., Creech H. C. and Soinila, S. O. “Evidence for chaos in spike trains of neurons that generate rhythmic motor patterns,” *Brain Research Bulletin*, vol. 21, pp. 529–538, 1988.
- [Pomeau and Manneville, 1980] Pomeau Y. and Manneville, P. “Intermittent transition to turbulence in dissipative dynamical systems,” *Commun. Math. Phys.*, vol. 74, pp. 189–197, 1980.
- [Pyragas, 1992] Pyragas, K. “Continuous control of chaos by self-controlling feedback,” *Phys. Lett. A*, vol. 170, pp. 421–428, 1992.
- [Selverston, 1976] Selverston, A. “A model system for the study of rhythmic behavior,” in J. C. Fentress (Ed.), *Simpler Networks and Behavior*, Sinauer, Sunderland, MA, pp. 83–98, 1976.

- [Skarda & Freeman, 1987] Skarda C., and Freeman, W. J. “How brain make chaos to make sense of the world,” *Behavioral and Brain Sciences*, vol. 10, pp. 161–195, 1987.
- [Strogatz & Stewart, 1994] Strogatz S. H., and Stewart, I. “Synchronization of rhythm in creatures,” *Scientific American*, vol. 269, no. 11, pp. 58–69, 1994.
- [Thiran, 1997] Thiran, P. *Dynamics and Self-Organization of Locally Coupled Neural Networks*, Presses Polytechniques et Universitaires Romandes, 1997.
- [Ueta et al., 2001] Ueta, T. Chen, G. and Kawabe T. “A simple approach to calculation and control of unstable periodic orbits in chaotic piecewise linear systems,” *International Journal of Bifurcation and Chaos*, Vol. 11, No. 1, pp. 215-224, Nov. 2001.
- [Ueta et al., 1997] Ueta, T., Tsueike, M., Kawakami, H., Yoshinaga, T. and Katsuta, Y. “A computation of bifurcation parameter values for limit cycles,” *IEICE Trans. Fundamentals*, vol. E80-A, pp. 1725–1728, 1997.
- [Vreeswijk, 2001] Vreeswijk, C. van. “Analysis of the asynchronous state in networks of strongly coupled oscillators,” *Physical Review Letters*, Vol. 84, No. 22, pp. 5110–5113, May 2001.
- [Wilson & Cowan 1973] Wilson, H. R. and Cowan, J. D. “A mathematical theory of the functional dynamics of cortical and thalamic nervous tissue,” *Kybernetik*, vol. 13, pp. 55–80, 1973.